Chapter 3

Harmonic Minimization in HC-MLI Using Modified Whale Optimization

3.1 Introduction

In this chapter, selective harmonics elimination pulse width modulation (SHE-PWM) technique has been employed through proposed modified whale optimization (MWO) for generating three phase, 11-level output voltage of hybrid cascaded hybrid multilevel inverter (HC-MLI) [111]. The MWO optimized three-phase HC-MLI enhances the performance in terms of harmonic content, rate of convergence and obtaining global optima quickly. In the proposed MWO optimized HC-MLI, capacitor voltage balance is made possible even at higher modulation indices using available redundant switching states of HC-MLI.

3.2 Mathematical Model of Whale Optimization Algorithm

Whale optimization (WO) algorithm is a naturally inspired meta-heuristic algorithm, which replicates the social behaviour of humpback whales [95], [96]. This algorithm is inspired by the bubble-net searching technique of humpback whales. The mathematical model of three main steps of hunting in WO; such as encircling prey, spiral bubble-net hunting and search for prey are discussed as follows:

3.2.1 Encircling Prey

The humpback whales encircle the prey and update their position towards the best search

agent. The humpback whales encircle the prey and update their position towards the best search agent using (3.1) and (3.2) are given as

$$D = \left|\vec{C} \cdot \vec{X}^*(j) - \vec{X}(j)\right| \tag{3.1}$$

$$\vec{X}(j+1) = \vec{X}^*(j) - \vec{A}.\vec{D} \tag{3.2}$$

where j is the current iteration, $\vec{X}$ indicates the position vector, $\vec{X}^*(j)$ is the position vector of the best solution till obtained, $\vec{A}$ and $\vec{C}$ are the coefficient vectors. The vector $\vec{A}$ is calculated as

$$\vec{A} = 2\vec{a} \cdot \vec{r} - \vec{a} \tag{3.3}$$

and vector $\vec{C}$ as

$$\vec{C} = 2.\vec{r} \tag{3.4}$$

where the value of $\vec{a}$ linearly decreases from [2, 0] and $\vec{r}$ is random vector between [0, 1].

3.3 Bubble-Net Attacking Method (Exploitation Phase)

In order to mathematically model the bubble-net behavior of humpback whales, two approaches are designed as follows:

3.3.1 Shrinking Encircling Mechanism

It is achieved by decreasing the value of coefficient vector $\vec{a}$ from 2 to 0 in (3.3) over the course of iterations. The vector $\vec{A}$ becomes greater than 1 or less than −1 in due course of time. By setting the values $\vec{A}$ in the range [−1, 1], the position of search agent can be expounded in between the original and the current best position of search agent. Fig. 3.1(a) shows the positions of humpback whale from current co-ordinate (X, Y) to best optimum co-ordinate (X^*, Y^*) in 2D space.

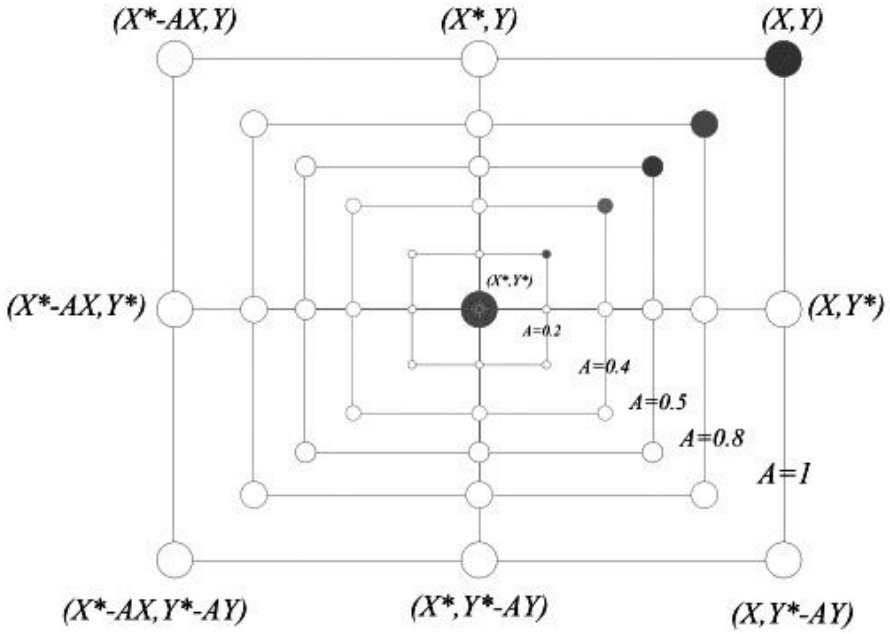

(a)

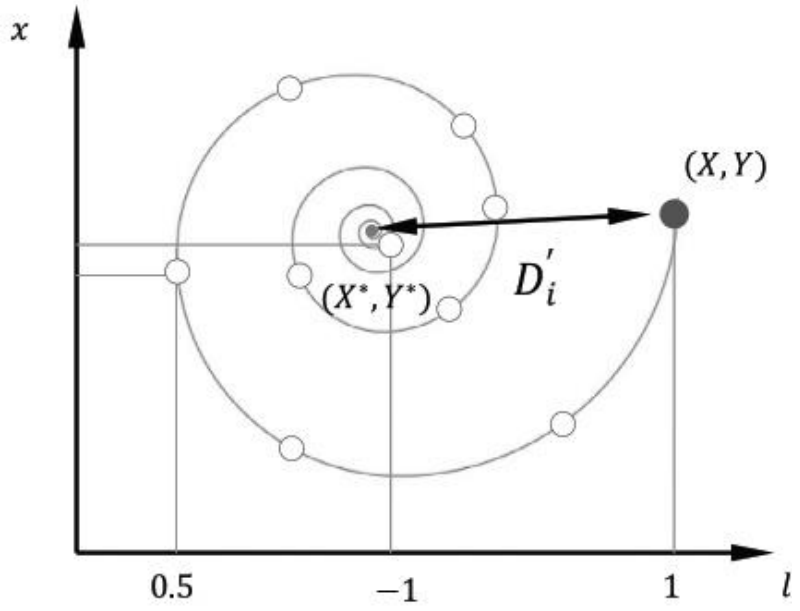

(b)

Fig. 3.1 Bubble-net search mechanism in WOA (X^* is the best solution obtained so far) [95]. (a) shrinking encircling mechanism. (b) spiral updating position.

3.3.2 Spiral Updating Position Mechanism

The spiral updating position mechanism calculates the distance between the whale located at (X, Y) and prey located at (X^*, Y^*) as shown in Fig. 3.1(b). A spiral equation is created between the position of whale and prey to mimic the helix-shaped movement of humpback whales as follows:

$$\vec{X}(j+1) = \vec{D}' e^{pq} \cdot \cos(2\pi q) + \vec{X}^*(j) \tag{3.5}$$

where $\vec{D}' = \vec{X}^*(j) - \vec{X}(j)$ specifies the distance of the i^{th} humpback whale to the search prey, p is a constant which outlines the shape of the logarithmic spiral, q is a random number in the interval [−1, 1] and r denotes a random number in the interval [0, 1].

Assuming, 50% probability to select either the shrinking encircling or the spiral technique, the mathematical model for updating the position of humpback whale is given as

$$\vec{X}(j+1) = \begin{cases} \vec{X}_P(j) - \vec{A}.\vec{D} & if\ r \leq 0.5 \\ \vec{D}' \cdot e^{pq} \cdot \cos(2\pi q) + \vec{X}^*(j) & if\ r \geq 0.5 \end{cases} \tag{3.6}$$

where $\vec{D}' = \vec{X}^*(j) - \vec{X}(j)$ specifies the distance of the i^{th} humpback whale to the search prey, p is a constant which outlines the shape of the logarithmic spiral, q is a random number in the interval [−1, 1] and r denotes a random number in the interval [0, 1].

3.3.3 Search for prey

The adaptation of $\vec{A}$ vector is exploited to search the prey. $\vec{A}$ becomes greater than 1 or less than −1 in due course of time to emphasize exploration for achieving global search. The mathematical model for search of prey is given as

$$D = \left|\vec{C} \cdot \vec{X}_{rand} - \vec{X}\right| \tag{3.7}$$

$$\vec{X}(j+1) = \vec{X}_{rand} - \vec{A}.\vec{D} \tag{3.8}$$

where $\vec{X}_{rand}$ is a random whale position vector.

3.4 Merits of WO Algorithm

WO algorithm has better performance as compared to reported optimization algorithms in terms of exploitation, exploration ability and ability to get rid of the local minima. In the initial step of the algorithm, the whales try to move randomly around each other using (3.5). In the next step, the whales update their positions rapidly and move along a spiral shaped route in the direction of the best path that has been found so far using (3.6). Since these two stages are completed independently and in half iteration each, WOA has inherent property to get rid of the local minima.

3.5 Limitation of WO Algorithm

The encircling mechanism in WO algorithm mostly focuses on the exploration in the search space. As a result, WO has less capability to jump out from local optima, in case it falls in it. The convergence rate and speed depend only on one control parameter *a* and it has an excessive impact on the performance of WO [96]. Hence, WO has poor convergence speed in both exploration and exploitation phases. A balancing formulation mechanism between exploration and exploitation is required.

3.6 Proposed Modifications in WO Algorithm

To improve the convergence speed in both exploration and exploitation phase and to avoid possible local optima stagnation during encircling mechanism, a local search algorithm, called chaotic search mechanism is combined with WO to enhance the rate of convergence and avoid it from being stuck at local optima [112]. The evolved method is named as modified WO (MWO) in this work. A proper balance between exploration and exploitation is necessary in MWO due to its stochastic nature. MWO balances the exploration by

modifying the position co-efficient to an exponentially decaying function. Generally, higher exploration of search space results in lower probability of local optima stagnation. More exploration causes higher randomness and will probably not give good optimization results. Basic exploration and exploitation prevent the algorithm from finding global optima and results poor rate of convergence. Therefore, there must be a balance between exploration and exploitation. The proper balance between exploration and exploitation guarantees accurate estimation of the global optima. In MWO, the transition between them is obtained by the adaptive values of *A* and *a*. The function which gives the exponential decay for *a* during the iterations is given as

$$a = 2\left(1 - \frac{m}{n}\right) \tag{3.9}$$

where *m* indicates the maximum number of iterations and *n* is the current iteration. The numbers of iterations used for exploration and exploitation are 60% and 40% respectively.

The theory of nonlinear chaos has widely been used in different applications in last decade [112]. Dynamical chaotic systems are able to control unsteady intermittent gestures. In basic WOA, search agents are distributed irregularly in the search space because of their random initializations. The irregular distributions might provide a better start of the algorithm. However, the lack of ergodicity makes the algorithm trapped in local optimum. WOA with chaotic search technique has been applied in this work for the improvement of search efficiency and the reduction of the possibility of being trapped at the local optima. The chaotic equation used in MWO is defined as

$$x_{j+1} = \mu . x_j \left(1 - x_j\right) \tag{3.10}$$

where x_j is a variable ($j = 0,1,2\cdots$) and μ is the control parameter.

The procedure of chaotic local search is described as

$$cx_j^{n+1} = \mu . cx_j^n \left(1 - cx_j^n\right) \tag{3.11}$$

where cx_j^n represents the chaotic variable. *n* represents the iteration number.

The procedures of MWO is depicted in Fig. 3.2 and listed as follows:

Step 1: Set $n = 0$ and map the decision variables x_j^n from the interval ($x_{\min, j}, x_{\max, j}$) to chaotic variables cx_j^n using

$$cx_j^{n+1} = \frac{x_j^n - x_{min,\, j}}{x_{max,\, j} - x_{min,\, j}} \tag{3.12}$$

Step 2: Determine the chaotic variables cx_j^{n+1} for the next iteration using 3.9.

Step 3: Convert the chaotic variables cx_i^{n+1} to decision variables x_j^{n+1} using

$$x_j^{n+1} = x_{min,\, j} + cx_j^{n+1}(x_{max,\, j} - x_{min,\, j}) \tag{3.13}$$

Step 4: The new solutions are evaluated with variables x_j^{n+1}.

Step 5: If the new solution achieves better performance or the maximum number of iterations is reached, take the new solution as chaotic local search; or else, modify $n = n + 1$ and go back to Step 2.

The procedure for explaining the optimisation problem using MWO is as follows:

Step 1: Initialise MWO parameters between upper and lower limits.

Step 2: Generate initial population randomly.

Step 3: Calculate fitness value of each whale in the population and sort it according to their fitness values to choose best fit search agent.

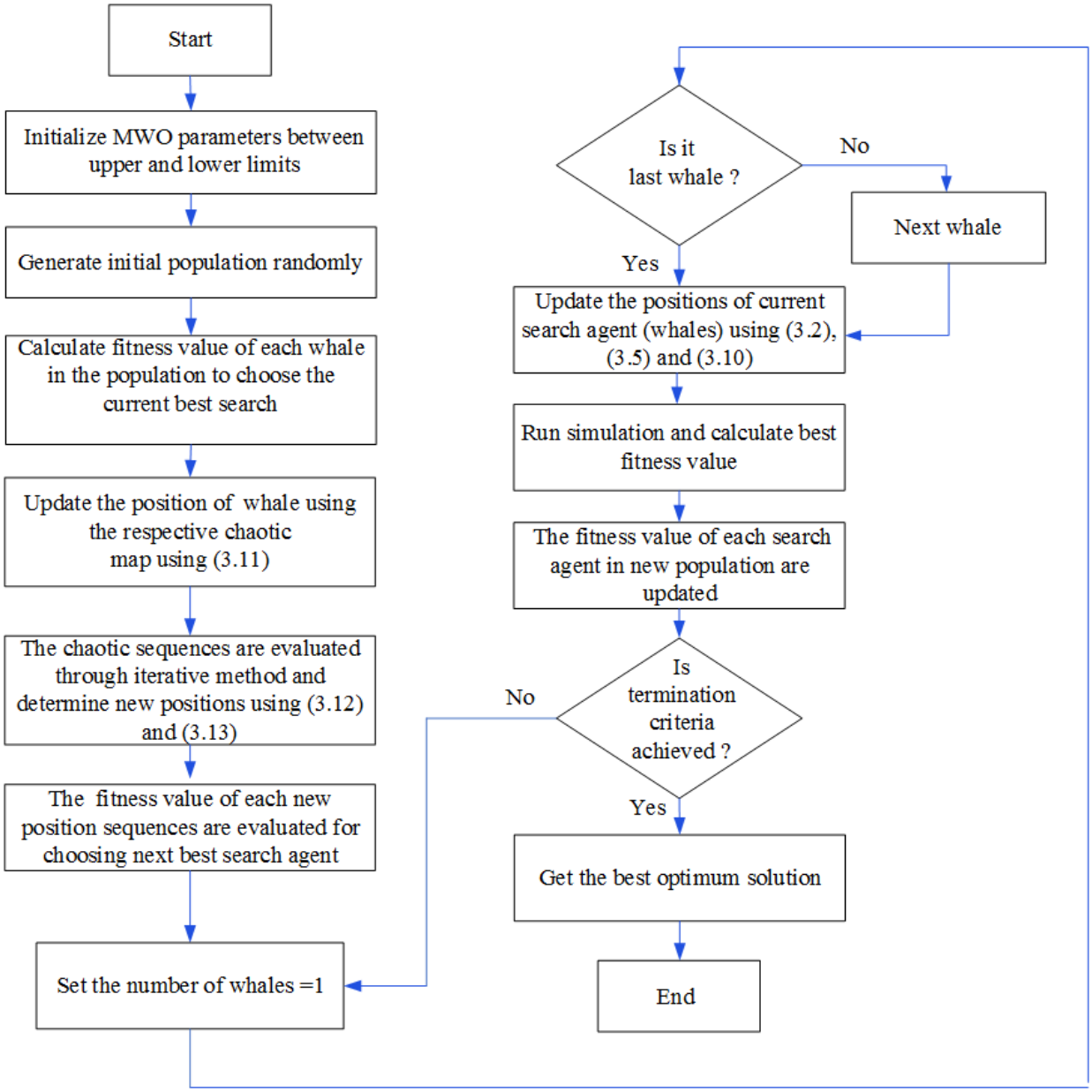

Fig. 3.2 Description of MWO algorithm.

Step 3: Calculate fitness value of each whale in the population and sort it according to their fitness values to choose best fit search agent.

Step 4: The position of whale is mapped into chaotic variables using (3.12).

Step 5: The chaotic sequences are evaluated through iterative technique and converted chaotic sequences represented as new positions using (3.11) and (3.13).

Step 6: The fitness of new position sequences is evaluated.

Step 7: Update co-efficient *A* and *C* in (3.3) and (3.4) and the parameter *a*, *q* and *r* in (3.7) and (3.6).

Step 8: For ($r < 0.5$)

If ($|A| < 1$), The position of the current search agent is updated using (3.2).

else ($|A| > 1$) Select a random search agent (X_{rand}) and the position of the current search agent is updated using (3.10).

Step 9: For ($r > 0.5$)

The position of the current search agent is updated by (3.5).

Step 10: Update the fitness values of each search agent till global optima is achieved.

Step 11: Check the boundary limit of the search agent.

3.7 Application of MWO Based SHE-PWM in HC-MLI

The proper objective function *f* is represented by the following mathematical equation

$$f = \min\left\{\left(100\frac{V_1^* - V_1}{V_1^*}\right)^4 + \frac{1}{5}\left(50 \times \frac{V_5}{V_1}\right)^2 + \frac{1}{7}\left(50 \times \frac{V_7}{V_1}\right)^2 + \frac{1}{11}\left(50 \times \frac{V_{11}}{V_1}\right)^2 + \frac{1}{13}\left(50 \times \frac{V_{13}}{V_1}\right)^2\right\} \quad (3.14)$$

subjected to

$$0 \leq \theta_1 \leq \theta_2 \ldots \theta_n < \frac{\pi}{2} \quad (3.15)$$

The main objective is to minimize (3.14) to maintain actual fundamental voltage component (V_1) close to the desired value (V_1^*) and to eliminate 5^{th}, 7^{th}, 11^{th} and 13^{th} harmonic components from the output voltage. From (3.14), it can be observed that harmonic

components are reversely weighted to their harmonic orders (1/5, 1/7, 1/11 and 1/13) in the fitness function to give more importance to eliminate lower order harmonics. The number of iterations and population size in the algorithm are chosen as 200 and 150 respectively. The algorithm starts with the random initialization of whales (switching angles) and the fitness of each whale is evaluated. Exponentially decaying position co-efficient balances exploration versus exploitation. The algorithm is run for different modulation indices till the termination criteria is achieved. The plot of switching angles against modulation index (m_a) is shown in Fig. 3.3. The graph of the value of fitness function versus m_a is shown Fig. 3.4.

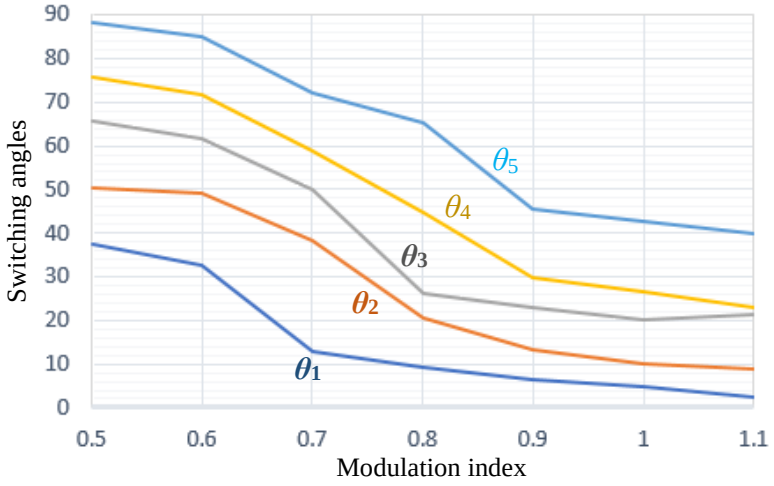

Fig. 3.3 Obtained switching angles at different m_a.

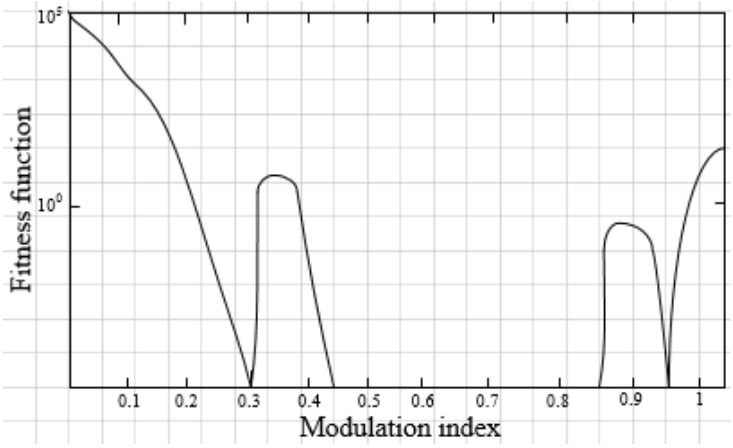

Fig. 3.4 Fitness function value versus m_a.

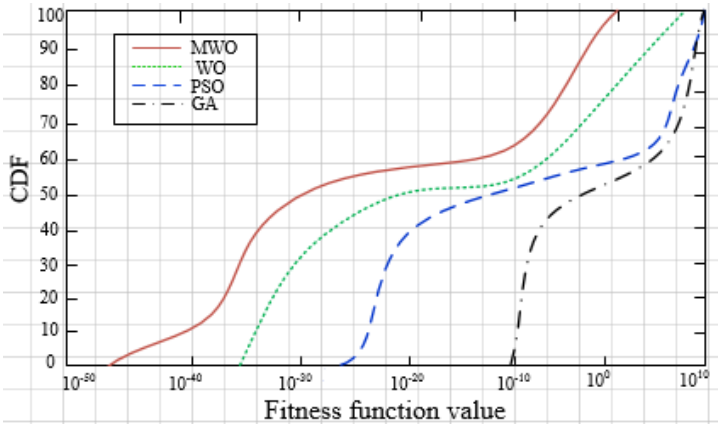

Fig. 3.5 Rate of convergence comparison of WO, PSO and GA algorithms.

In order to compare the convergence rates, the comparison plot of cumulative distribution function (CDF) versus optimum fitness values for algorithms MWO, WO, PSO and GA are shown in Fig. 3.5. It can be observed from Fig. 3.5 that MWO has the highest CDF value, which confirms its higher probability of convergence as compared to other algorithms. Fig. 3.6(a)-10(d) show the magnitude of 5th, 7th, 11th and 13th harmonic components of the output line voltage with respect to fundamental component (V_5/V_1, V_7/V_1, V_{11}/V_1 and V_{13}/V_1) versus modulation index. It can be observed that 5th, 7th, 11th and 13th harmonic components are lowest for MWO and highest for GA.

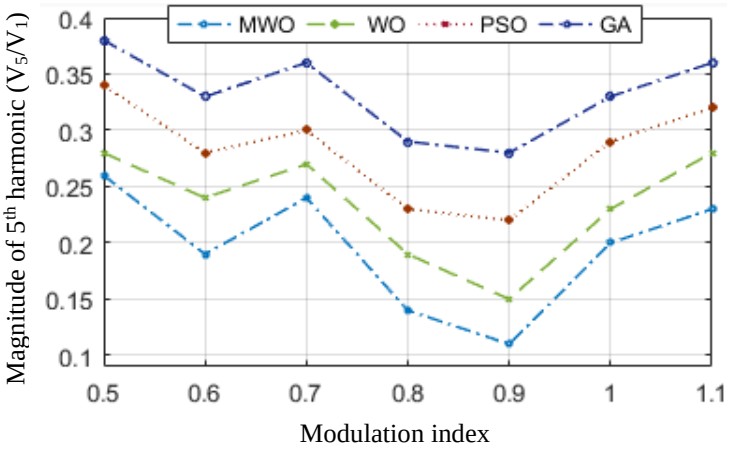

(a)

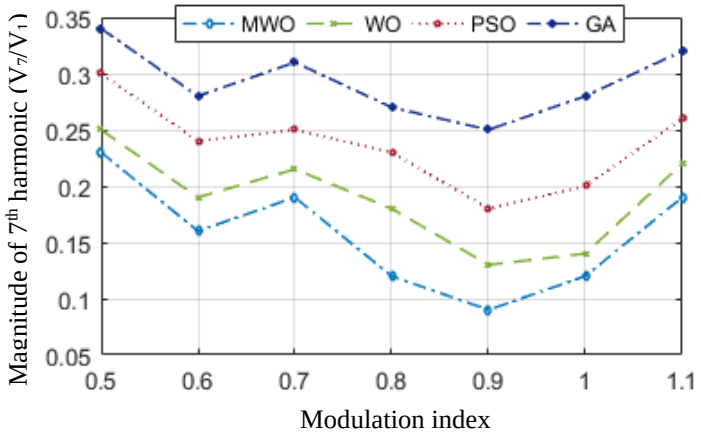
MWO
WO
PSO
GA
Magnitude of 7th harmonic (V7/V1)
0.35
0.3
0.25
0.2
0.15
0.1
0.05
0.5
0.6
0.7
0.8
0.9
1
1.1
Modulation index

(b)

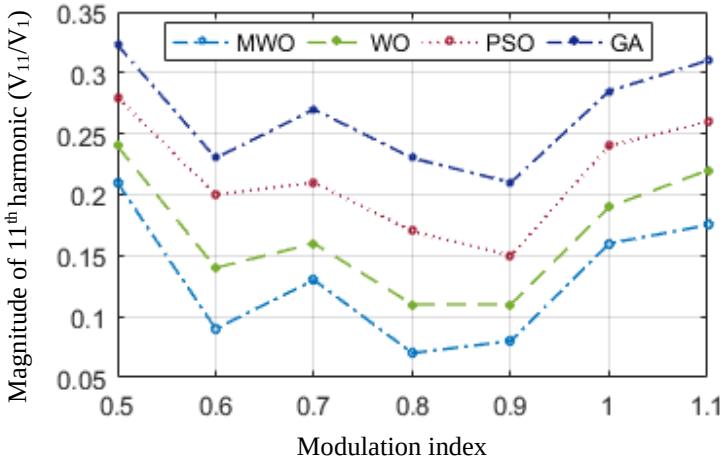
MWO
WO
PSO
GA
Magnitude of 11th harmonic (V11/V1)
0.35
0.3
0.25
0.2
0.15
0.1
0.05
0.5
0.6
0.7
0.8
0.9
1
1.1
Modulation index

(c)

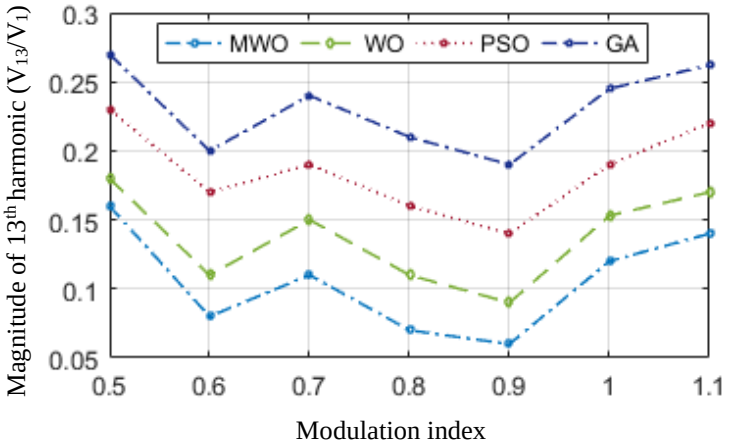
MWO
WO
PSO
GA
Magnitude of 13th harmonic (V13/V1)
0.3
0.25
0.2
0.15
0.1
0.05
0.5
0.6
0.7
0.8
0.9
1
1.1
Modulation index

(d)

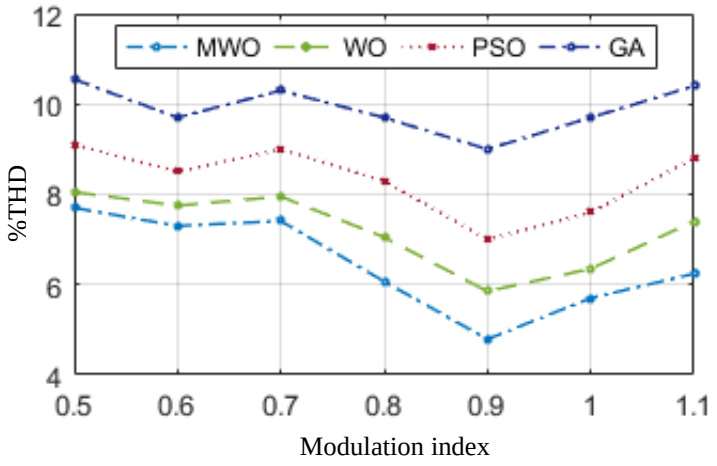

(e)

Fig. 3.6 Comparison between harmonics of different algorithms (GA, PSO, WO and MWO). (a) Magnitude of 5th harmonic. (b) Magnitude of 7th harmonic. (c) Magnitude of 11th harmonic. (d) Magnitude of 13th harmonic. (e) %THD of GA, PSO, WO and MWO.

Table 3.1
Parameters of MWO, WO, GA and PSO
No. of Iteration=200 and Population size =100 at (m_a=0.7)

Parameters	MWO	WO	PSO	GA
Fitness value	$6.7X10^{-30}$	$4.7X10^{-10}$	$5.3X10^{-2}$	0.0624
Convergence rate	Very high	High	High	Low
Rank of convergence	1	2	3	4
Computational time (sec)	1.312	1.168	1.712	3.146

Fig. 3.6(e) shows the of % total harmonic distortion (THD) of output line voltage comparison of MWO, WO, PSO and GA at different modulation indices. It can be observed %THD is least in case MWO among the algorithms compared. The comparison of fitness values and convergence rate of different algorithms are given in Table 3.1. So, the computational time required for digital MWO is slightly complicated in comparison to WO because this

algorithm is a combination of global exploration and local exploitation. It can be inferred from Table 3.1 that the computational time for MWO is less as compared to GA and PSO algorithms. However, the proposed MWO gives improved results than WO, PSO and GA in terms of possibility of attaining global optima, higher rank of convergence, higher fitness value and harmonic content for the same population size and number of iterations.

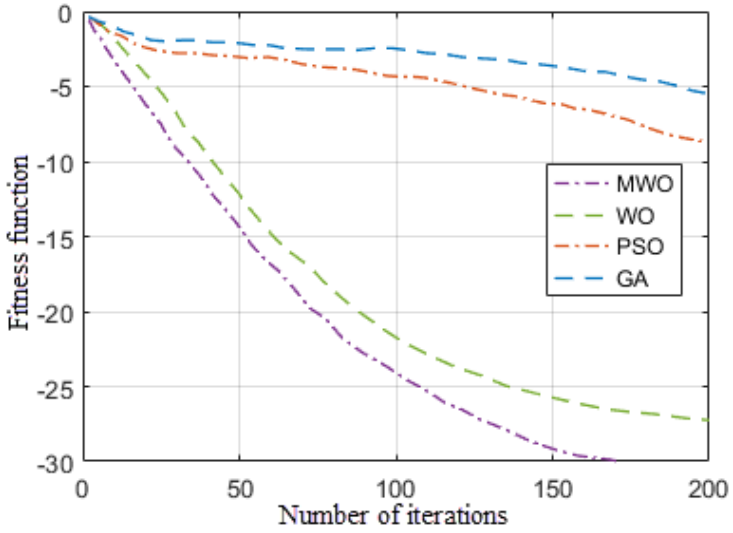

(a)

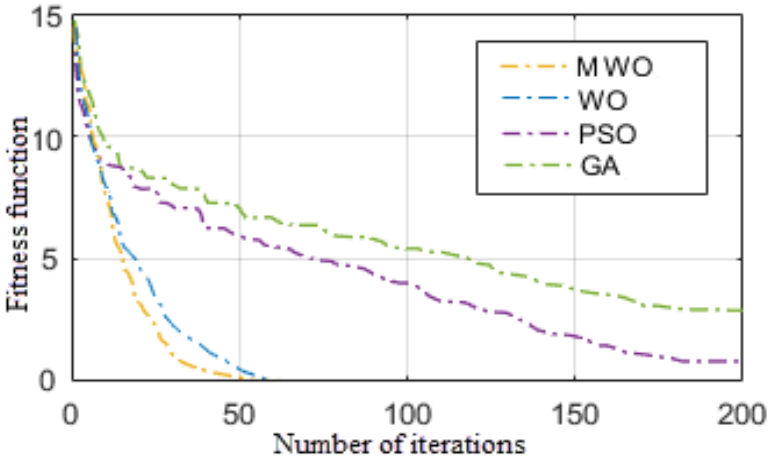

(b)

Fig. 3.7 Convergence plots of MWO, WO, PSO and GA. (a) Sphere function. (b) Rosenbrock function.

In order to compare different algorithms, standard test functions are used to measure the convergence speed. The Sphere and Rosenbrock functions are used to measure the convergence speed or the number of iterations required for convergence [113]. For Sphere and Rosenbrock function dimension, range and minimum value of function ($f_{\min}$) are taken as 30, [-100, 100], 0 and 30, [-30, 30], 0 respectively. The plot of fitness function versus number of iterations required are shown in Fig. 3.7(a) and 11(b) respectively. It can be concluded from Fig. 3.7 that MWO finds global solution more effectively with lesser number of iterations as compared to WO, PSO and GA. Hence, the convergence speed of MWO is fastest among the different algorithms compared.

3.8 Simulation Studies

In order to verify the proposed work, three-phase, 11-level HC-MLI has been simulated in MATLAB/Simulink environment using proposed MWO algorithm.

3.8.1 Working at $m_a = 0.6$

From Fig. 3.3, the switching angles that are obtained are $\theta_1 = 32.43$, $\theta_2 = 49.21$, $\theta_3 = 61.45$, $\theta_4 = 71.68$ and $\theta_5 = 85.31$. The output voltage waveform V_0 of HC-MLI and the waveform of capacitor voltage V_{cap} are shown in Fig. 3.8(a). The capacitor voltage is balanced at 30 V.

3.8.2 Working at $m_a = 1.1$

Similarly, for $m_a = 1.1$, the switching angles are obatained are $\theta_1 = 2.41$, $\theta_2 = 8.67$, $\theta_3 = 21.35$, $\theta_4 = 23.12$ and $\theta_5 = 39.84$. These switching angles will not satisfy the capacitor voltage criteria. Hence, in order to balance the capacitor, a third harmonic voltage is injected as discussed in section 2.6.2 of chapter 2. Output voltage V_0 and capacitor voltage V_{CAP} without and with capacitor balance are shown in Fig. 3.8(b) and 3.8(c) respectively. The average value of the capacitor voltage also gets balanced at 30 V for higher modulation index.

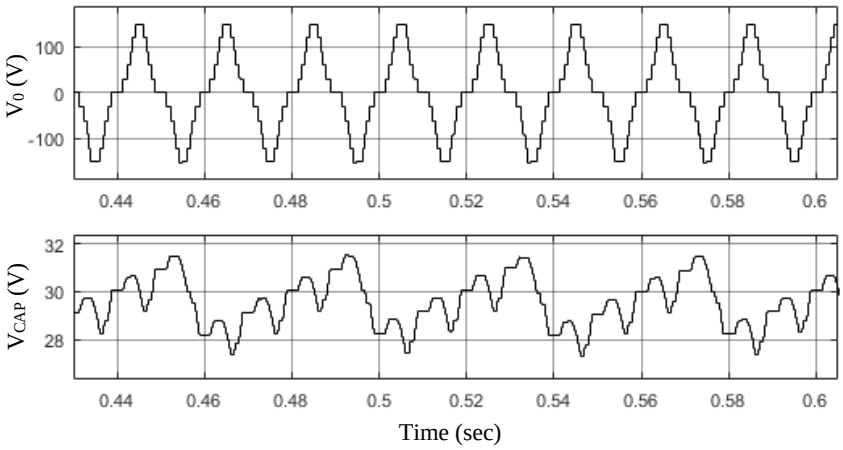

(a)

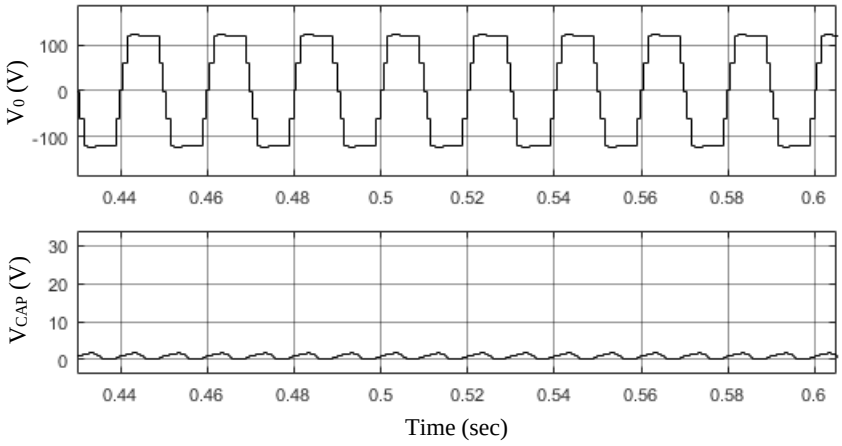

(b)

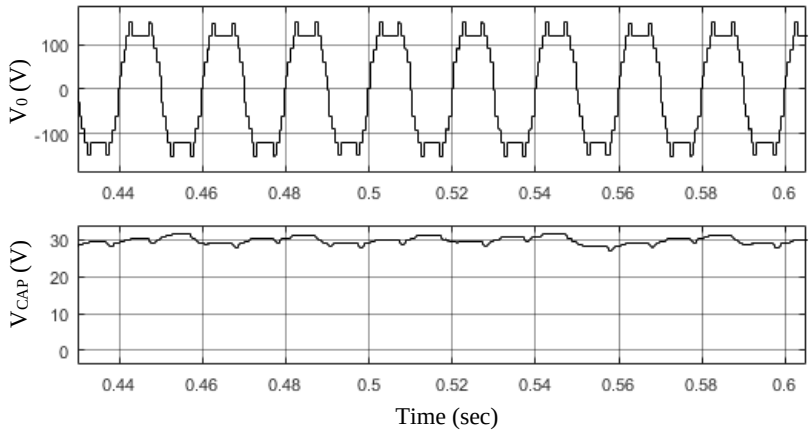

(c)

Fig. 3.8 Simulation results of MWO optimized HC-MLI for capacitor voltages. (a) V_0 and V_{CAP} for modulation index (m_a) = 0.6. (b) V_0 and V_{CAP} for m_a = 1.1 in case of unbalanced condition of capacitor. (c) V_0 and V_{CAP} for m_a = 1.1 at balanced capacitor voltage.

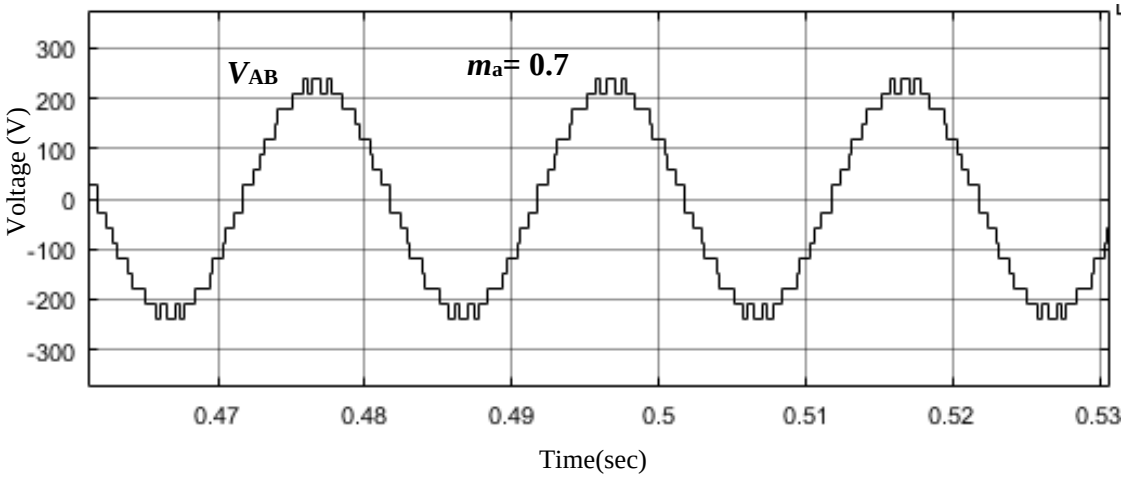
V_{AB}
m_a= 0.7
Voltage (V)
Time(sec)

(a)

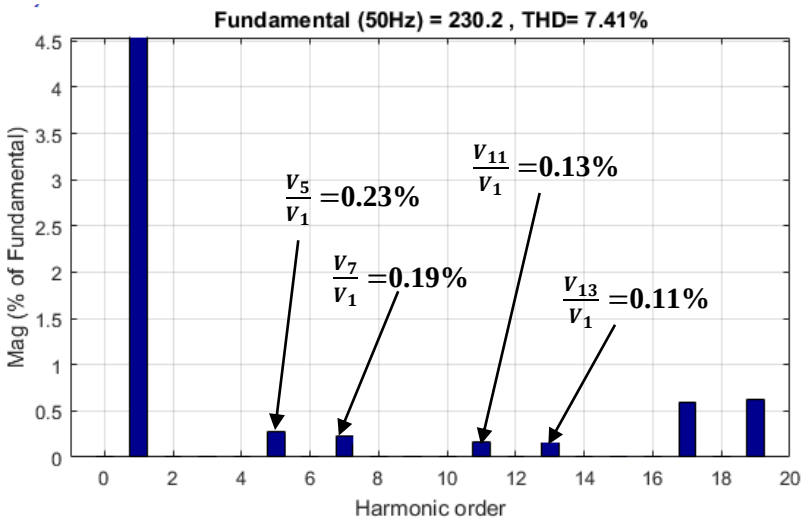
Fundamental (50Hz) = 230.2 , THD= 7.41%
Mag (% of Fundamental)
Harmonic order
$\frac{V_5}{V_1}$ =0.23%
$\frac{V_7}{V_1}$ =0.19%
$\frac{V_{11}}{V_1}$ =0.13%
$\frac{V_{13}}{V_1}$ =0.11%

(b)

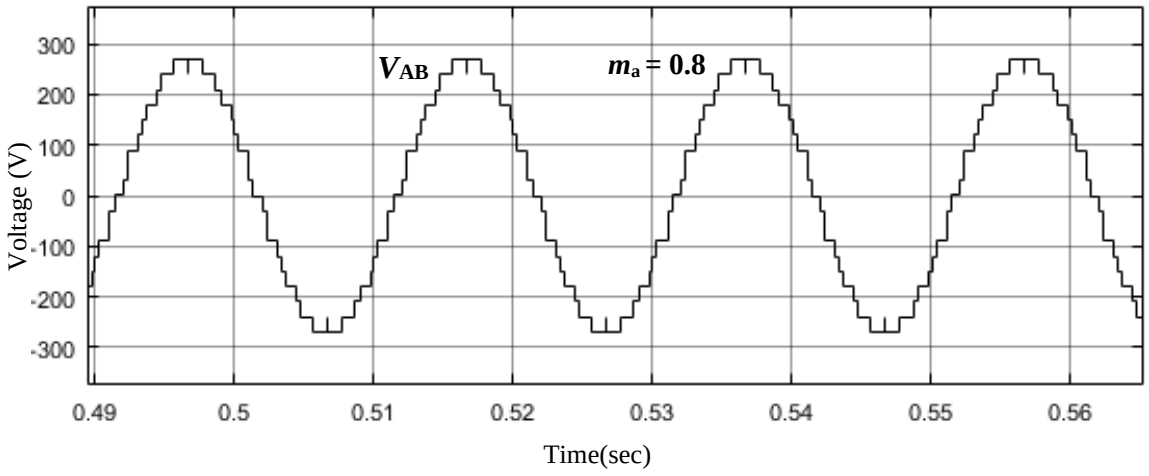
V_{AB}
m_a = 0.8
Voltage (V)
Time(sec)

(c)

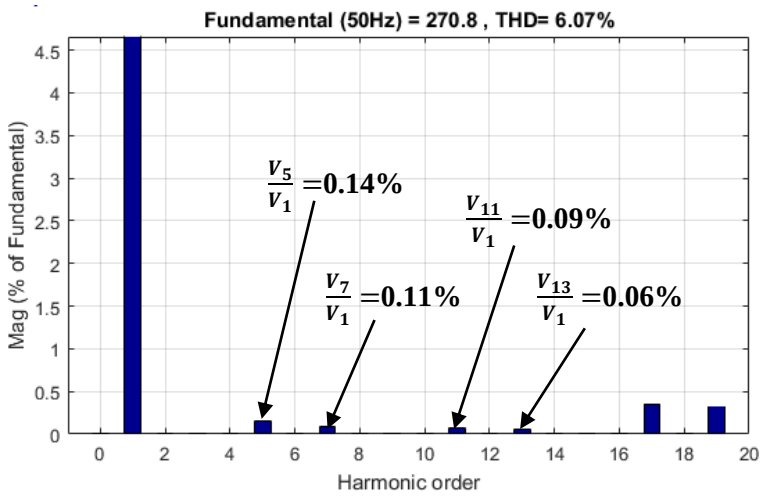

(d)

Fig. 3.9 Simulation results of HC-MLI (Line voltages and harmonic spectrum). (a) Output voltage V_{AB} at $m_a = 0.7$. (b) Harmonic spectrum at $m_a = 0.7$. (c) Output voltage V_{AB} at $m_a = 0.8$. (d) Harmonic spectrum at $m_a = 0.8$.

The output line voltage (V_{AB}) and their corresponding harmonic spectrums depicting magnitude of lower order harmonics (5^{th},7^{th}, 11^{th} and 13^{th}) are shown in Fig. 3.9. The simulation results of output line voltage and its harmonic analysis for $m_a = 0.7$ are shown in Fig. 3.9(a) and (b) and for $m_a = 0.8$ are shown in Fig. 3.9(c) and (d) respectively.

3.9 Experimental Verification

A 1.5 kW laboratory prototype is used to verify the performance of the proposed MWO optimized three-phase, 11-level HC-MLI, as shown in Fig. 2.24 of chapter 2. The phase voltages (V_A, V_B and V_C) of HC-MLI for resistive load at $m_a = 0.6$ are shown in Fig. 3.10(a) and measured as 88.52 V. The balancing of capacitor voltage at higher modulation index is investigated experimentally. The phase A voltage (V_A) at $m_a = 1.1$ is shown in Fig. 3.10(b) and three phase voltages (V_A, V_B and V_C) are shown in Fig. 3.10(c) and measured as 111.62 V. The capacitor voltage is balanced at 30 V. Hence, it confirms the balancing of capacitor voltage at higher m_a. For *R-L* load (R=12 Ω and L= 37 mH), the output voltage V_A and output

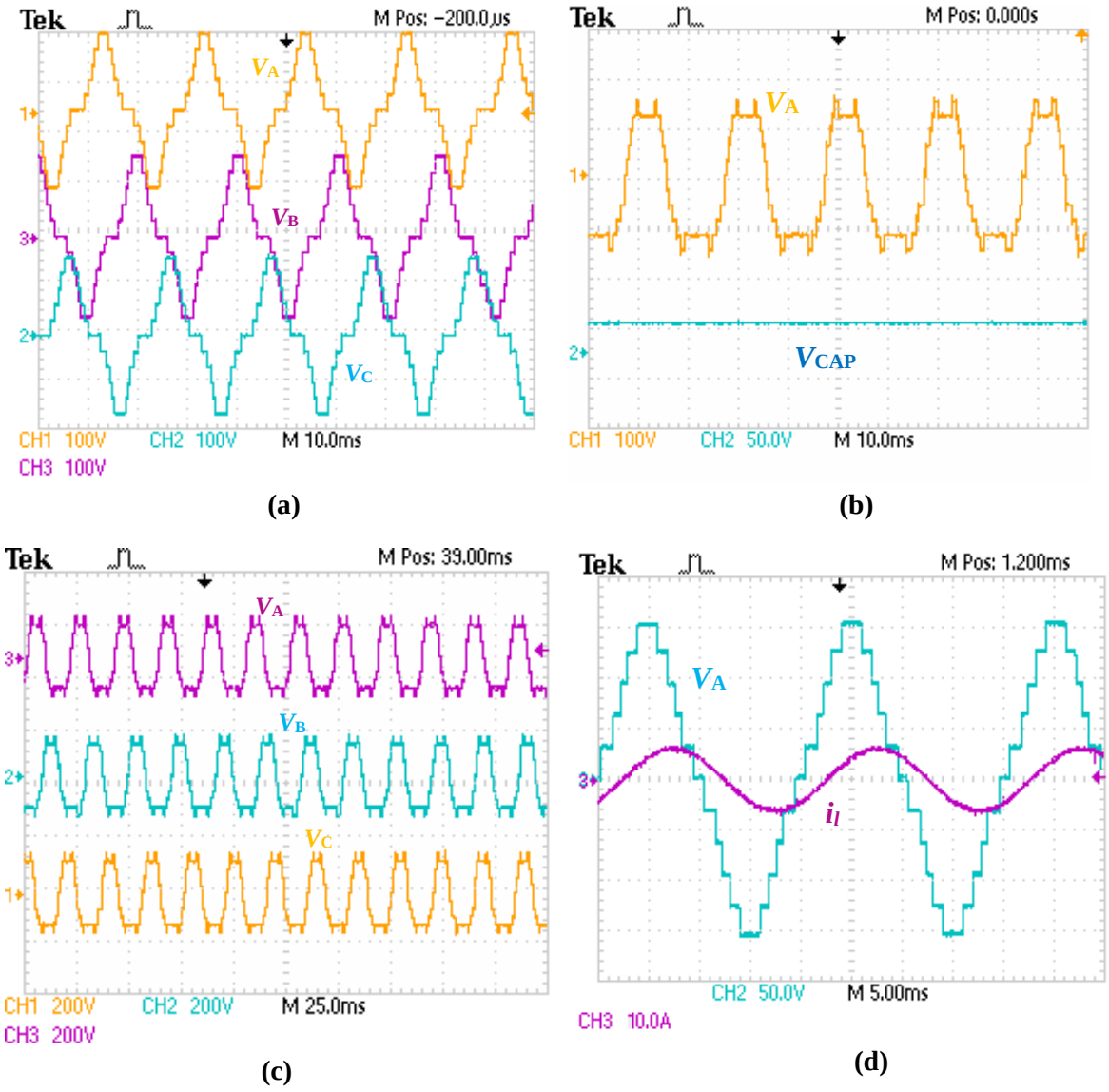

Fig. 3.10 Experimental results (Phase voltages).
(a) V_A, V_B and V_C for $m_a = 0.6$. (b) V_A for $m_a = 1.1$. (c) V_A, V_B and V_C for $m_a = 1.1$. (d) i_l for inductive load (R=12 Ω and L= 37 mH) for m_a = 0. 6.

current I_L are shown in Fig. 3.10(d). The line-line voltage (V_{AB}) of the MWO optimized HC-MLI at $m_a = 0.7$ is shown in Fig. 3.11(a) and measured as 174 V. The harmonic analysis of (V_{AB}) at $m_a = 0.7$ is shown in Fig. 3.11(b). It can be observed from Fig. 3.11(b) that the lower order harmonics such as 5^{th}, 7^{th},11^{th} and 13^{th} are reduced. Similarly, the line voltage (V_{AB}) for $m_a = 0.8$ is shown in Fig. 3.11(c) and its corresponding harmonic spectrum is shown in Fig. 3.11(d).

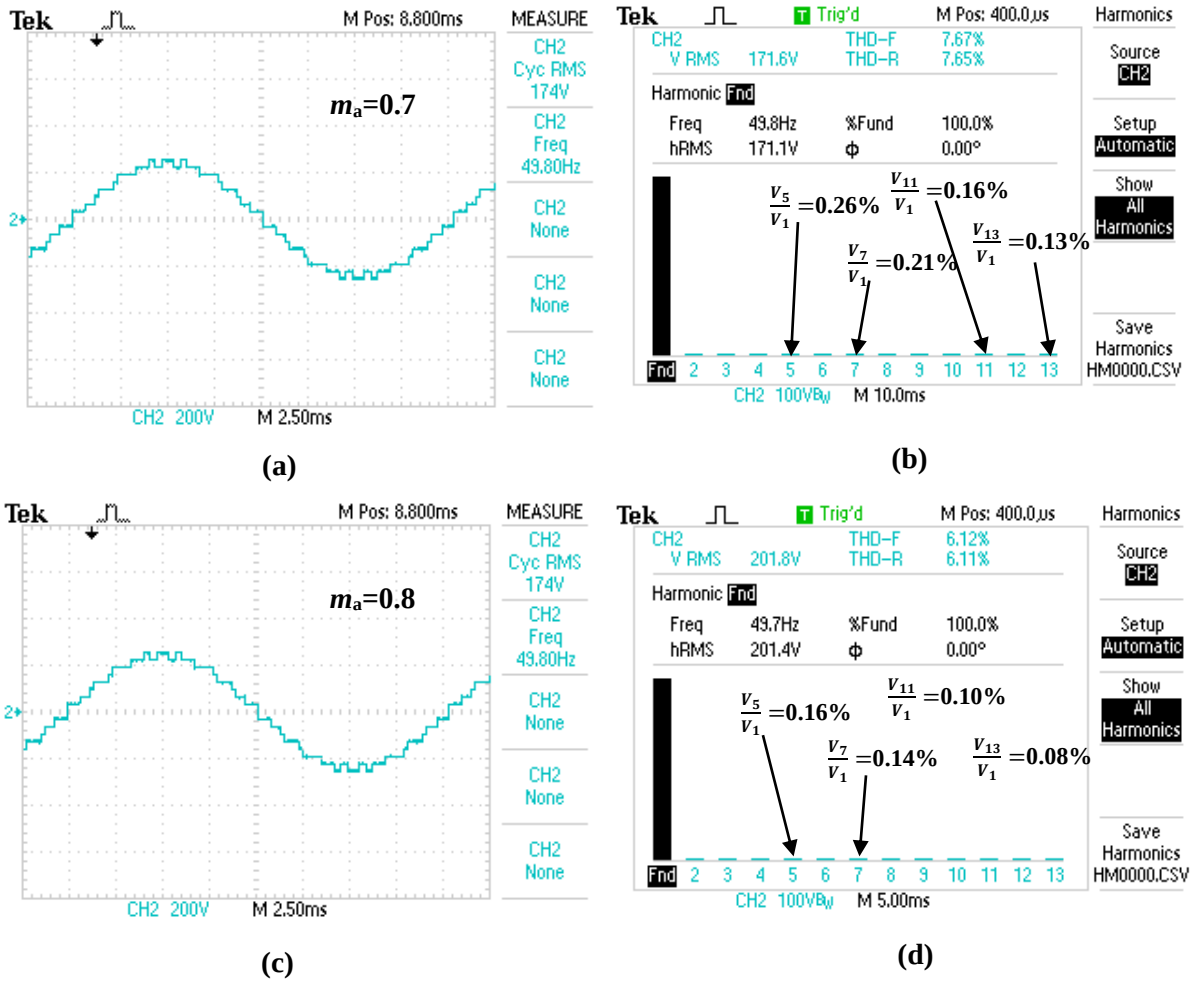

Fig. 3.11 Experimental results of HC-MLI (Line voltages and harmonic spectrums).
(a) Line-line voltage (V_{AB}) for m_a = 0.7. (b) Spectrum of harmonic analysis of V_{AB} for m_a 0.7 (c) Line-line voltage (V_{AB}) for m_a 0.8. (d) Spectrum of harmonic analysis of V_{AB} for m_a 0.8.

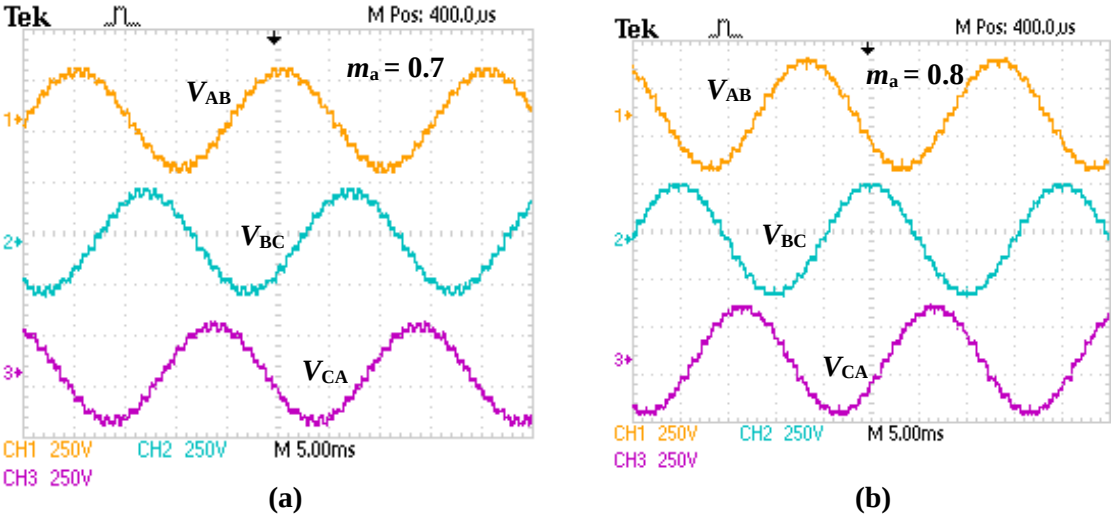

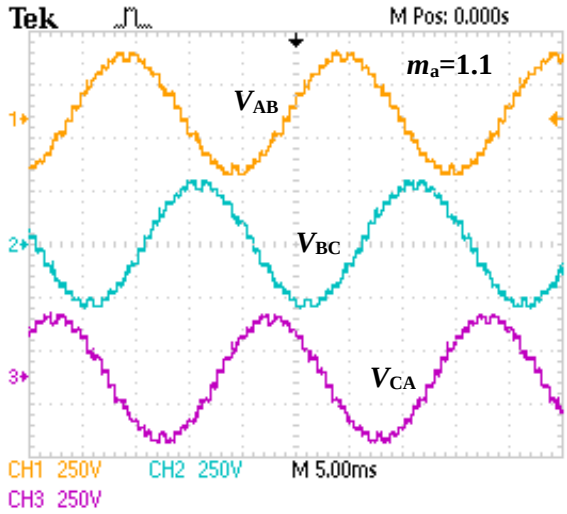

(c)

Fig. 3.12 Three-phase experimental results of HC-MLI.
(a) Line-line voltage (V_{AB}, V_{BC} and V_{CA}) for m_a = 0.7. (b) Voltage (V_{AB}, V_{BC} and V_{CA}) for m_a = 0.8. (c) Voltage (V_{AB}, V_{BC} and V_{CA}) for m_a = 1.1.

The harmonic magnitudes are within the IEEE Std 519-2014 [110]. Experimental results of line-line voltages (V_{AB}, V_{BC} and V_{CA}) at m_a = 0.7, 0.8 and 1.1 are shown in Fig. 3.12(a)-(c). The comparison of experimental %THD of proposed MWO with other reported optimization algorithms such as WO, PSO and GA is given in Table 3.2.

Table 3.2
Experimental %THD Comparison of Different Algorithms

Modulation index	%THD (MWO)	%THD (WO)	%THD (PSO)	%THD (GA)
0.5	7.41	8.57	10.27	13.87
0.6	6.53	7.12	9.21	12.35
0.7	6.69	7.53	9.73	12.86
0.8	6.05	6.98	7.42	11.32
0.9	4.81	5.18	6.05	10.85
1	5.83	6.17	7.09	9.87
1.1	6.24	7.71	7.71	8.05

3.10 Conclusion

In this chapter, MWO optimized three-phase, 11-level HC-MLI is presented using SHE-PWM. The use of adaptive position co-efficient vector and exponentially decaying function

in MWO gives improved results as compared to WO. In MWO, chaotic local search technique efficiently takes care of possible local optima strategy and enhances the convergence rate as compared to GA, PSO and WO. MWO also helps to obtain the global optima quickly as compared to other reported evolutionary algorithms and effectively eliminates lower order harmonics from the output voltage of HC-MLI. Moreover, the proposed MWO control strategy balances the capacitor voltage even at higher modulation index by exploiting the redundancies of HC-MLI. Simulation and experimental studies are carried out to demonstrate steady state and dynamic performance of the proposed MWO optimized three-phase HC-MLI. In order to further improve the performance in terms of speed of convergence and harmonic content, modified grey wolf optimization (MGWO) algorithm has been used in HC-MLI in the next chapter.